Published in final edited form as:
Circ Res. 2008 September 26; 103(7): 710–716. doi:10.1161/CIRCRESAHA.108.181388.

Syx, a RhoA guanine exchange factor, is essential for angiogenesis *in vivo*

Maija K. Garnaas[1], **Karen L. Moodie**[3], **Miao-liang Liu**[3], **Ganesh V. Samant**[1], **Keguo Li**[1], **Ruth Marx**[2], **Jay M. Baraban**[2], **Arie Horowitz**[3,*], and **Ramani Ramchandran**[1,@,*]

[1]Medical College of Wisconsin, Department of Pediatrics, CRI Developmental Vascular Biology Program, Translational and Biomedical Research Center, CRI C3420, 8701 Watertown Plank Road, P.O. Box 26509, Milwaukee, WI 53226, USA

[2]John Hopkins University, Solomon H Snyder Department of Neuroscience, Baltimore, MD 21205, USA

[3]Dartmouth Medical School, One Medical Center Drive, HB 7504, Lebanon, NH 03756, USA

Abstract

Rho GTPases play an important and versatile role in several biological processes. In this study, we identified the zebrafish ortholog of the mammalian Rho A guanine exchange factor (GEF), Synectin-binding GEF (Syx), and determined its *in vivo* function in the zebrafish and the mouse. We found that *Syx* is expressed specifically in the vasculature of these organisms. Loss-of-function studies in the zebrafish and mouse point to a specific role for Syx in angiogenic sprouting in the developing vascular bed. Importantly, vasculogenesis and angioblast differentiation steps were unaffected in *syx*-knockdown (KD) zebrafish embryos, and the vascular sprouting defects were partially rescued by the mouse ortholog. Syx KD *in vitro* impairs vascular endothelial growth factor-A (VEGF-A) induced endothelial cell migration and angiogenesis. We have also uncovered a potential mechanism of endothelial sprout guidance in which Angiomotin (Amot), a component of endothelial cell junctions, plays an additive role with Syx in directing endothelial sprouts. These results identify Syx as an essential contributor to angiogenesis *in vivo*.

Keywords

vascular; zebrafish; PDZ; knockdown; intersomitic vessels

INTRODUCTION

Two distinct processes – vasculogenesis and angiogenesis – characterize vascular development in vertebrates [1, 2]. During vasculogenesis, vessels form *de novo* from endothelial cell (ECs) precursors, or angioblasts, that coalesce at the midline to form lumenized tubes. Once primary vessels have formed, ECs sprout from preexisting vasculature to form secondary vessels via angiogenesis. ECs proliferate, migrate and differentiate to form mature vasculature. Directed cell migration is necessary for angiogenesis and is governed in part by Rho-family GTPases, including RhoA, Cdc42, and Rac1 [3]. Activation of Rho GTPases at the cell periphery by Rho GEFs[4] leads to remodeling of the actin cytoskeleton and consequently to cell migration [5].

@**Corresponding authors**: Ramani Ramchandran[1] and Arie Horowitz[3], **Phone**: 414-955-2387, **Fax**: 414-955-6325, rramchan@mcw.edu.
*Equal contribution

Recently, a novel Rho-GEF, Synectin-binding RhoA exchange factor (Syx), also named GEF720 PLEKHG5, and Tech [6], was identified by yeast two-hybrid analysis using Synectin as bait [7] (M. Simons, personal communication). The mouse Syx ortholog is expressed as two splice variants that differ by only two C-terminal amino acid residues [8]. Full-length Syx1 contains a Postsynaptic density 95, Disk large, Zona occludens-1 (PDZ) motif [9] required for Syx1's interaction with Synectin and localization to the plasma membrane. The shorter variant, Syx2, lacks the PDZ motif and is diffusely distributed in the cytoplasm. Syx1 augments ECs migration and tube formation whereas Syx2 does not [8]. The first report on Syx localized it to band 1p36, in the distal region of human chromosome 1[6]. This chromosomal region is rearranged in several types of cancer suggesting that Syx may be involved in malignant transformation. The same report detected high expression levels of Syx in the brain and the heart, both highly vascularized organs [6]. More recently, a missense mutation in Syx was linked with a degenerative motor neuron disease [10]. Given the well-known similarities between signaling pathways in the nervous and vascular systems [11], the expression and functions of Syx in both system is not surprising. The most recent annotations of the human genome classified Syx as belonging to a 7-member family of GEFs (PLEKHG5: pleckstrin homology domain containing, family G (with Rho-GEF domain) member 5). The functions of the other members of this family are still unknown.

To investigate Syx's function in vertebrate vascular development, we identified the Syx ortholog in zebrafish and performed whole mount *in situ* hybridization (ISH). *Syx* is expressed in the dorsal aorta (DA) and intersomitic vessels (ISVs). *Syx* vascular expression is recapitulated in mammals where the mouse Syx protein is observed in the DA and coronary vessels. Both gain and loss-of-function analyses in zebrafish demonstrated specific defects in ISVs sprouting. Injection of mouse *syx* mRNA partially rescued these defects, suggesting evolutionary conservation of Syx function. Furthermore, we found that Syx and Angiomotin, a regulator of ECs migration [12–14], act additively during angiogenesis. These results implicate for the first time a Rho-GEF that function specifically in vertebrate angiogenesis *in vivo*.

MATERIALS AND METHODS

Zebrafish stocks and reagents

Zebrafish were maintained at 28.5°C [15] under MCW guidelines (protocol no. 312-06-2). Mating was carried out at 28.5°C, and embryos were staged according to established protocols [16]. Morpholinos MO1 and MO2 were designed by Gene Tools (Philomath, OR) to target a *syx* intron-exon boundary and the *syx* ATG start codon, respectively. MO1, AGCTGTTTCT*GTGT*GGCCTGCTGA; MO2, CATGCCTTCGCCAATAGAACATCGT. Splice site nucleotides are italicized. The Amot MO sequence has been published previously [14].

Whole mount *in situ* hybridization

WT embryos were grown in 0.003% phenylthiourea until the desired staged, fixed overnight at 4°C in 4% paraformaldehyde (PFA), dechorionated, and stored in 100% methanol at −20° C until use. Whole mount *in situ* hybridization was performed as described[17] using *etsrp*, *fli*, *flk*, *flt4*, *grl*, and *syx* probes. DIG-labeled sense and antisense *syx* probes were transcribed from a *XmnI*-linearized vector containing 541 bp of *syx* using T7 and SP6 RNA polymerases, respectively. Zebrafish *syx* cDNA used to make the RNA probes was obtained from Open Biosystems (Clone: 65260512, Huntsville, AL).

Tg *(fli: EGFP)*$^{clom39-/+}$ zebrafish and *Cre/loxP syx*$^{-/-}$ mouse generation

Refer to Online text.

Micro-computed tomography (μCT)

We used wild type (WT) and *syx* knockout (KO) mice fixed at end-diastole. The mice were anesthetized by ketamine/xylazine, heparinized, and euthanized by perfusion with citric KCl. After a PBS wash, mice were fixed by perfusion with 4% paraformaldehyde. A MV-132 (Flow-Tech) contrast medium was infused into the coronary system via the aorta, or into the renal arteries. The hearts were imaged by a General Electric eXplore Locus SP apparatus at a resolution of 13 μm, and the vasculature was reconstructed by Microview(GE) software.

RESULTS

Two zebrafish NCBI sequences (accession numbers XM_686228.1 and XM_686228.2, encoding 1143 AA and 858 AA proteins, respectively) match mouse and human Syx, which are 1073 and 1091 AA, respectively. Amino acids 14–858 of the shorter zebrafish sequence (Online Figure IB) are identical to AA 297–1141 of the longer sequence (Online Figure IA), suggesting that alternative start sites generate two proteins with different N-termini. We have also detected multiple isoforms of *syx* by RT-PCR (data not shown). The 1143 AA Syx protein contains Rho-GEF (Dbl-homologous, DH) (Online Figure IA, black arrows) and Pleckstrin homology domains (Online Figure IA, grey arrows), and a PDZ-binding motif (ASEV) at its C-terminus (Fig. 1A). Its amino acid sequence is 60% and 59% homologous to mouse (Online Figure IA) human orthologs (data not shown), respectively. Human *syx* is located on chromosome 1, which is syntenic to linkage group 11 where zebrafish *syx* is located. Based on synteny and conserved domain structure, we conclude that the zebrafish *syx* gene reported here is the ortholog for human *syx*.

Syx is expressed in the developing zebrafish and mouse vasculature

To determine the spatial and temporal expression of *syx*, we performed whole mount ISH on zebrafish embryos. A *syx* antisense digoxigenin (DIG)-labeled RNA probe was generated from an expressed sequence tag (Open Biosystems, Clone ID 65260512), which spans 541 bp of the 5’ end of the longer *syx* transcript and 203 bp of the shorter transcript. *Syx* is expressed maternally in 4-cell stage embryos (Online Figure IIA, B). Expression continues in blastomeres at 3 hours post fertilization (hpf) (Online Figure IIC) and is ubiquitous in 12 somite (som) embryos (Online Figure IID). At 18 som (Online Figure IIE), *syx* expression is fairly ubiquitous and is observed along the midline (Online Figure IIF). Starting at 23–24 hpf (Fig. 1B and 1C), *syx* transcripts are restricted to axial vessels (Fig. 1B, black arrow). At 24–26 hpf, (Figs. 1D and 1E), *syx* expression is noted in the ISVs (Fig. 1E, white asterisks). We also checked for Syx expression in mammalian tissue by probing cryosections of E12.5 mouse embryos with anti-Syx (a custom-made antibody) (Fig. 1F) and anti-Platelet endothelial cell adhesion molecule 1 (PECAM-1/CD31) (Fig. 1H), an EC marker. We found that Syx is expressed in the endothelium of the aorta, coronary vessels, and endocardium of the atria and left ventricle (Fig. 1F and 1G). Syx was also detected in the ascending aorta (data not shown) but not in the vena cava, suggesting that Syx is an artery-specific protein. Both zebrafish and mouse share Syx aorta expression.

The endocardial expression of Syx in the mouse prompted us to investigate whether *syx* is differentially expressed in the cardiovascular genetic mutant *cloche* (*clo*) in zebrafish [18], which lacks the endocardial layer. Real time PCR analysis for *syx* showed that *syx* levels are reduced in $clo^{-/-}$ embryos compared to WT embryos (Online Figure IIG). We injected *syx* mRNA into Tg(*fli1*: EGFP)$^{clom39-/-}$ embryos where the Tg(*fli1*: EGFP) line has been crossed into the $clo^{m39+/-}$ background and observed for rescue of *clo* defects. *Syx* mRNA-injected embryos from Tg(*fli1*: EGFP)$^{clom39+/-}$ mating pairs did not show significant differences in Mendelian ratios for edema or gain of the vascular marker *fli1*-EGFP compared to embryos from

uninjected mating pairs (Online Figure IIH), suggesting that *syx* may be indirectly affected in the *cloche* mutant.

Knockdown of *syx* perturbs ISVs development in the zebrafish

We designed two morpholinos (MOs) to knockdown (KD) *syx* transcripts in zebrafish. MO efficacy is shown in Online Figure III and the results discussed in Online text. The effect of *syx* KD on zebrafish vascular development was analyzed in transgenic fish carrying an endothelial-specific promoter of vascular endothelial growth factor receptor-2 (*vegfr2 or flk)* 19 or friend leukemia integration factor-1 (*fli1)* 20, which drive expression of green fluorescent protein (GFP) specifically in the vasculature. Transgenic embryos were injected with 8 ng of MO1 or MO2 at 1-cell stage, and vessel development was monitored via fluorescence microscopy. By 24 hpf, uninjected embryos showed ISVs that migrated dorsally between somites (Fig. 2A, asterisk). In MO1-injected embryos, the ISVs were truncated, and the leading front of the tip cell was blunt (Fig. 2C, asterisk). Occasionally, one or two ISVs were completely absent (Fig. 2C). At 28 hpf, the growth of ISVs in MO1-injected embryos remained stagnant (Fig. 2D, asterisk), while those of uninjected embryos continued to grow to form the dorsal longitudinal anastomotic vessel (Fig. 2B, asterisk). A second MO targeting the ATG translational start site, MO2 (8 ng), also caused growth arrest of ISVs (Figs. 2E and 2F, asterisk). Quantification of MO-injected embryos at 24 hpf (Fig. 2G) revealed that 62% of Tg (*fli1*: EGFP) and 42% of Tg(*flk*: G-RCFP) MO1-injected embryos displayed ISVs defects compared to only 10% and 7% of their age-matched uninjected siblings, respectively. 30% of MO2-injected Tg(*fli1*: EGFP) embryos had ISVs growth defect (Fig. 2G), suggesting some variability in MO efficacy, which is expected since MO1 targeted both forms of the *syx* transcript, whereas MO2 targeted only the long form.

To determine gastrulation delays upon MO injection, we performed ISH with the gastrulation marker *myod* in MO1-injected (Online Figure IIIE) and uninjected (Online Figure IIID) embryos at 24 hpf. We observed no difference in *myod* expression patterns between samples, suggesting that the vascular phenotype caused by MO1 injection did not result from delayed gastrulation.

To investigate if vascular defects originated at a developmental stage that preceded ISVs sprouting, we performed ISH with *etsrp*, an early angioblast marker [21]. At 14 hpf (Figs. 3A–D) or 18 hpf (Fig. 3E–H) all the sample groups displayed normal *etsrp* expression pattern. To confirm the phenotypes observed in Tg(*fli1*: EGFP) embryos, we performed ISH with the *fli* probe at 24 hpf in uninjected (Fig. 3I) and MO-injected (Figs. 3J and 3K) embryos. We observed a darker *fli* staining of the DA in MO1-injected embryos, similar to the more intense GFP signal in the Tg(*fli1*: EGFP) zebrafish (Fig. 2C), suggesting the presence of more number of ECs. In MO1-injected embryos at 24 hpf, secondary fli^+ ISVs sprouting from the DA appeared defective and were truncated (Fig. 3J, white asterisk) or misguided (Fig. 3J, white arrowhead). Some ISVs ends were marked by darker staining in both MO1 and MO2-injected embryos similar to the swollen ends of GFP-expressing ISVs (asterisks in Figs. 3J and 3K). Quantification at 24 hpf (Fig. 3M) showed that 11% of the MO1-injected embryos had no more than five ISVs, while 42% had truncated ISVs. In MO2-injected embryos, 2% had no ISVs, 5% had less than five ISVs, and 44% had truncated ISVs. Similar results were observed in MO-injected flk^+ embryos at 22 hpf (Online Figure IIIF). The most common ISVs defect was growth arrest rather than complete absence, suggesting that *syx* primarily affected ISVs directional migration, and not the initial sprouting from the DA.

syx gain of function also affects ISVs development

To determine whether *syx* gain-of-function can complement *syx* loss-of-function, we injected capped mouse *syx* mRNA and performed ISH using *etsrp*, *flk*, and *fli* probes. At 14 hpf,

etsrp-probed *syx* RNA-injected (Fig. 3D) embryos appeared normal, showing angioblast patterning comparable to uninjected and the MO1 and MO2-injected embryos. Similarly, at 18 hpf we observe no vascular defects in *flk* expression (data not shown). In *syx* mRNA injected *fli* ISH embryos, vascular defects were observed at 24 hpf where ISVs showed blunt ends (Fig. 3L, asterisk) mimicking the phenotype of the MO-injected embryos at the same time point. These result suggest that gain and loss-of-function are not complementary but similar.

syx does not affect artery vs. vein (A/V) specification

In 24 hpf syx KD (Fig. 3J and 3K) or *syx* mRNA injected (Fig. 3L) embryo, we observed an intense blue staining in DA for *fli* ISH. In particular, fli^{+} region in *syx* mRNA-injected embryos was expanded into both the DA and posterior cardinal vein (PCV) (Fig. 3L). Therefore, we checked the arterial marker *gridlock* (*grl*) [22] at 24 hpf and the venous marker *flt4*23 at 30 hpf to determine whether A/V differentiation is affected in *syx*-KD embryos. ISH with *grl* and *flt4* antisense probes showed no difference in staining in MO or RNA-injected embryos when compared to uninjected embryos (data not shown), suggesting that *syx* is not required for angioblast differentiation. Collectively, our ISH results confirm the transgenic embryo data that *syx* plays an exclusive role in directing ISVs sprout growth from the DA.

Vascular defects are partially rescued by *syx* gene complementation

To demonstrate MO specificity, we co-injected Tg(*fli1*: EGFP) embryos with *syx* sense mRNA and MO1 and compared them to embryos injected with MO1 alone. Initially, we performed rescue experiments with 100 pg of *syx* mRNA and observed no rescue in MO1-injected embryos (data not shown). Subsequently, we increased the dose of mRNA to 150 or 200 pg and observed a concomitant reduction in ISVs defects in co-injected embryos when compared to MO1-injected embryos (Fig. 3N). However, we were only able to partially rescue the phenotype with the two mRNA doses (12% and 15% rescue, respectively). When the amount of mRNA was further increased to 300 pg, the number of rescued embryos was reduced to 6%, suggesting a saturation effect. These results indicate that ISVs sprouting requires a precise level of *syx* expression. Since the injection of mouse *syx* mRNA partially rescued the endogenous *syx* knockdown effects in zebrafish, we conclude that *syx* function is conserved across vertebrate species.

Disruption of *syx* expression in the mouse causes angiogenic defects

To study Syx function in mammals, Cre loxP $syx^{-/-}$ mice were generated and crossed with germ-line Cre mice, which results in a global disruption of *syx* expression. $Syx^{-/-}$ mice were viable up to at least 12 months and appeared grossly normal. Since *syx* is expressed in the cardiac and vascular tissue in the mouse (Fig. 1F), and *syx* KD zebrafish shows defective ISVs, we imaged the coronary and kidney arterial systems by micro-computed tomography (μCT) of WT and $syx^{-/-}$ mice. Both the coronary (Fig. 4A) and kidney (Fig. 4B) arterial systems of the $syx^{-/-}$ mice were sparser than those in the WT mouse. On close examination, these systems appeared to be deficient in small diameter vessels, but the major coronary and kidney arteries are present. This defect is analogous to the *syx* KD zebrafish, where the dorsal aorta was intact but ISVs were truncated (Figs. 2D and 2F). In order to quantify the coronary arterial defect, we used μCT images to measure the total volume of the contrast medium infused into the coronary arteries of the WT and $syx^{-/-}$ mice. We found that the ratio between the volumes of the $syx^{-/-}$ and WT coronary arterial systems was 0.75±0.11 (n=5, p=0.002).

Since the μCT technique cannot image capillaries due to the viscosity of the contrast medium, we probed sections of WT and $syx^{-/-}$ myocardia by histochemistry. The images clearly show that the density of capillaries in the $syx^{-/-}$ was significantly lower than in the WT myocardium (Fig 4C). Together with the μCT images, these results demonstrate that the $syx^{-/-}$ mouse harbors a vascular defect affecting multiple organs. The major arteries are intact, but the growth

of secondary arteries and capillaries was defective. We conclude that the defect is specific to the angiogenic stage of arterial development, without affecting arteriogenesis similar to the vascular defect in zebrafish treated with syx MOs. The similarity of secondary vessel defects in the zebrafish and the mouse suggest that *syx*'s function in angiogenesis is highly conserved across evolution.

Angiomotin and *syx* function additively during ISVs sprouting

The recently published *angiomotin* (*amot*) KD phenotype in zebrafish [14] is strikingly similar to that of *syx*. To determine if *amot* and *syx* regulate ISVs sprouting additively, we co-injected half doses of MOs for each gene (4 ng each) or each MO alone (4 ng or 8 ng) into Tg(*flk*:GRCFP) fish and compared the images of the vascular system in each sample. The ISVs of uninjected embryos track along the somites (Fig. 5A), but the ISVs of 4 ng of *syx* MO (Fig. 5B) or *amot* MO (Fig. 5C) injected embryos were stunted. When *amot* and *syx* MOs were co-injected at 4 ng each, truncation of ISVs sprouts (Fig. 5D, white asterisk) was more severe than those in embryos injected with a single MO. In some cases, the ISVs in embryos co-injected by *amot* and *syx* MOs were completely absent (Fig. 5E, white asterisk). Injection of *syx* or *amot* MO (4 ng) alone resulted in approximately half (23% and 28%, respectively) as many ISVs-defective embryos (Fig. 5I) as injection of double the dose (8 ng) of each MO (60% and 45%, respectively; Fig. 5I). In co-injected (4 ng *syx* MO + 4 ng *amot* MO) samples, the number of embryos with defective ISVs doubled compared to embryos injected by 4 ng of a single type of MO (50%, Fig. 5I). High power images of ISVs in uninjected embryos at 28 hpf revealed elongated filopodia protruding out of their tip cells (Fig. 5F), whereas the tip cells of ISVs in embryos injected by either *syx* MO (Fig. 5G) or by both *syx* and *amot* MOs (Fig. 5H) were round and devoid of filopodia. Given the known ISVs defect caused by *robo4* KD in zebrafish [17], we sought to determine the effect of co-injecting *syx* and *robo4* MOs.. We did not observe an additive effect between *robo4* and *syx* KDs (data not shown), suggesting that Syx and Robo4 do not share the same signaling pathway.

Angiomotin is thought to be involved in regulating ECs migration [12] similar to Syx [8], and is known to bind multi PDZ domain protein 1 (MUPP1), a large scaffold protein containing 13 PDZ domains [24]. We were able to co-immunoprecipitate MUPP1 and Syx1, but not Syx2 in ECs expressing each splice isoform fused to yellow fluorescent protein (Online Figure IVA). This result shows that Syx1 binds MUPP1 via its PDZ binding motif. The zebrafish ortholog of MUPP1 is likely, therefore, to functionally couple Amot and Syx1, accounting for the genetic interaction we observed between the two proteins.

Syx KD impairs ECs migration and angiogenesis in response to VEGF-A

VEGF-A is a major agonist of angiogenesis [25]. Since the vascular defects in the $syx^{-/-}$ mouse and in *syx*-KD zebrafish were angiogenic in nature, we tested the effect of silencing *syx* expression on ECs vessel formation, namely VEGF-A_{165} induced migration and *in vitro* tube formation. Transfection by *syx* siRNA significantly depleted Syx and reduced EC migration under basal conditions and in response to VEGF-A_{165} (Fig. 6A). The tubular network formed by ECs transfected with *syx* siRNA, either with or without VEGF-A_{165} was sparser than the network formed by cells transfected with control siRNA, indicating that Syx depletion impaired angiogenesis (Fig. 6B). However, *syx* siRNA endothelial cells did not show a difference in invasive behavior compared to control siRNA cells to either VEGF or serum stimulus indicating no function for Syx in invasion (Online Figure IVB). These results indicate that Syx has an essential role in specific steps of angiogenesis such as EC migration, in agreement with our previous results [8].

DISCUSSION

This study identifies the function of a novel Rho-GEF, Syx, in vascular development *in vivo*. We report three important findings. First, *syx* is specifically expressed in the vasculature of teleosts and mammals. Second, gain- and loss-of-function analyses show that *syx* plays a specific role in orchestrating directional migration of endothelial sprouts during vertebrate angiogenesis. Third, a novel-signaling axis between *syx* and *angiomotin* necessary for proper patterning of angiogenic vessels has been uncovered.

Vessel patterning in vertebrates is a complex process that involves the formation of primary axial vessels by vasculogenesis and the sprouting of secondary vessels by angiogenesis. This study focuses on the angiogenic mechanism of ISVs sprouting. Syx has been identified as a novel RhoA-specific GEF [7], which contributes to ECs migration *in vitro* 8. This function of Syx is consistent with previously published reports suggesting an important role for Rho GTPases in axon and endothelial tip cell guidance [26, 27].

We have extended the ECs expression profile of *syx* to mouse and zebrafish vessels. In both species, *syx* is expressed in the vasculature and in zebrafish the expression is almost exclusive to the DA and emerging sprouts. Since we did not detect *Syx* expression in the zebrafish PCV and in the mouse vena cava, it is likely that the Syx is specifically involved in arterial angiogenesis.

In the mouse, global disruption of the *syx* gene was accompanied by a significant reduction in the density of secondary arteries and of capillaries in the heart. We observed a similar reduction in the density of secondary arteries of the kidneys. Though we have not characterized additional vascular beds, we suspect that the angiogenic defect in the $syx^{-/-}$ mouse is likely to extend to all tissues and organs. Given the pivotal function of Syx in ECs migration [8], it is surprising that vascular defects in the $syx^{-/-}$ mouse and the *syx* KD zebrafish are not severe. In vascular development, isoform specific function of signaling molecules is frequently confined to specific developmental stages. For example, in zebrafish, the KDRa isoform of the VEGF-A receptor is specifically involved in arterial, but not in vein development, while KDRb, is dispensable for vascular development [28]. Therefore, functional redundancy across isoforms may partly explain this issue. Syx itself has multiple splice variants and moreover Syx is one isoform of a 7-member family of RhoA GEFs. Therefore, multiple back-ups exist in the system in which case syx must be tightly regulated.

Two lines of evidence suggest that maintaining optimal levels of *syx* is critical for directional migration of ISVs sprouts. First, both KD and overexpression of *syx* resulted in similar phenotypes. In both experiments, ISVs had sprouting defects, suggesting that ISVs growth requires a strict balance of guidance cues. When there is either a deficiency or overabundance of guidance molecules, the ISVs stall until a proper migratory path is established. These results mimic those observed for *robo4* 17, though we did not find evidence for a genetic interaction with *syx*. Second, in our complementation experiment study we injected mouse *syx* mRNA together with the *syx*-MO1 to demonstrate MO specificity and evolutionary conservation of *syx* function. Because 100 pg of *syx* mRNA did not rescue MO-induced vascular defects, we increased the dose of mRNA to 150 and 200 pg and saw a proportional increase in rescued embryos. However, when the dose of mRNA was increased to 300 pg, the percent of rescued embryos declined. These results also suggest that *syx* levels have to be maintained within a particular range to maintain proper vascular patterning.

A recent study demonstrated that *amot* KD caused ISVs defects phenotypically similar to *syx*'s [14]. In the current study, we found that *syx* and *amot* function additively to regulate ISVs sprouting. The genetic interaction between *amot* and *syx* is accounted for, at least in part, by

the coupling of the corresponding proteins via the adaptor protein MUPP1 ([24] and Online Figure IV). Both Amot and Syx are involved in mediating ECs migration in response to VEGF ([14] and Fig. 6A) further substantiating the functional cooperation between these proteins. The inhibitory effect of Syx depletion on *in vitro* ECs migration and tube formation in response to VEGF-A provides a potential molecular mechanism to explain the angiogenic defects in the $syx^{-/-}$ mouse and the *syx* KD zebrafish. The genetic interaction between Amot and Syx implies that the role of Syx in VEGF-A-induced angiogenesis is part of a more complex scenario involving additional signaling pathways. The binding of Syx to MUPP1, a component of tight junctions, [24, 29], and its presence in these junctions (data not shown) suggest a putative functional link between the association of Syx with tight junctions and its involvement in cell migration.

Supplementary Material

Refer to Web version on PubMed Central for supplementary material.

Abbreviations footnote

Amot, angiomotin
A/V, artery vs. vein
DA, dorsal aorta
GEF, guanine exchange factor
GFP, green fluorescent protein
hpf, hours post fertilization
ISVs, intersomitic vessels
KO, knockout
μCT, micro-computed tomography
MOs, morpholinos
PCV, posterior cardinal vein
MUPP1, multi PDZ domain protein 1
PDZ, Postsynaptic density 95, Disk large, Zona occludens-1
Syx, Synectin-binding GEF
VEGF, vascular endothelial growth factor
WT, wild type

ACKNOWLEDGEMENTS

The authors declare no competing financial interest. R. R is a recipient of National Cancer Institute (NCI) Scholar Award. This study was supported by National Institutes of Health grant HL67960 (A.H), by an American Heart Association Scientist Development Grant (M.L.), and by seed funds from the Children's Research Institute at the Medical College of Wisconsin (R.R.), Milwaukee.

REFERENCES

1. Risau W. Differentiation of endothelium. Faseb J 1995;9:926–933. [PubMed: 7615161]
2. Risau W, Flamme I. Vasculogenesis. Annu Rev Cell Dev Biol 1995;11:73–91. [PubMed: 8689573]
3. Fukata M, Nakagawa M, Kaibuchi K. Roles of Rho-family GTPases in cell polarisation and directional migration. Curr Opin Cell Biol 2003;15:590–597. [PubMed: 14519394]
4. Erickson JW, Cerione RA. Structural elements, mechanism, and evolutionary convergence of Rho protein-guanine nucleotide exchange factor complexes. Biochemistry 2004;43:837–842. [PubMed: 14744125]
5. Lamalice L, Le Boeuf F, Huot J. Endothelial cell migration during angiogenesis. Circ Res 2007;100:782–794. [PubMed: 17395884]

6. De Toledo M, Coulon V, Schmidt S, Fort P, Blangy A. The gene for a new brain specific RhoA exchange factor maps to the highly unstable chromosomal region 1p36.2–1p36.3. Oncogene 2001;20:7307–7317. [PubMed: 11704860]
7. Gao Y, Li M, Chen W, Simons M. Synectin, syndecan-4 cytoplasmic domain binding PDZ protein, inhibits cell migration. J Cell Physiol 2000;184:373–379. [PubMed: 10911369]
8. Liu M, Horowitz A. A PDZ-binding motif as a critical determinant of Rho guanine exchange factor function and cell phenotype. Mol Biol Cell 2006;17:1880–1887. [PubMed: 16467373]
9. Hung AY, Sheng M. PDZ domains: structural modules for protein complex assembly. J Biol Chem 2002;277:5699–5702. [PubMed: 11741967]
10. Maystadt I, Rezsohazy R, Barkats M, Duque S, Vannuffel P, Remacle S, Lambert B, Najimi M, Sokal E, Munnich A, Viollet L, Verellen-Dumoulin C. The nuclear factor kappaB-activator gene PLEKHG5 is mutated in a form of autosomal recessive lower motor neuron disease with childhood onset. Am J Hum Genet 2007;81:67–76. [PubMed: 17564964]
11. Carmeliet P, Tessier-Lavigne M. Common mechanisms of nerve and blood vessel wiring. Nature 2005;436:193–200. [PubMed: 16015319]
12. Bratt A, Birot O, Sinha I, Veitonmaki N, Aase K, Ernkvist M, Holmgren L. Angiomotin regulates endothelial cell-cell junctions and cell motility. J Biol Chem 2005;280:34859–34869. [PubMed: 16043488]
13. Wells CD, Fawcett JP, Traweger A, Yamanaka Y, Goudreault M, Elder K, Kulkarni S, Gish G, Virag C, Lim C, Colwill K, Starostine A, Metalnikov P, Pawson T. A Rich1/Amot complex regulates the Cdc42 GTPase and apical-polarity proteins in epithelial cells. Cell 2006;125:535–548. [PubMed: 16678097]
14. Aase K, Ernkvist M, Ebarasi L, Jakobsson L, Majumdar A, Yi C, Birot O, Ming Y, Kvanta A, Edholm D, Aspenstrom P, Kissil J, Claesson-Welsh L, Shimono A, Holmgren L. Angiomotin regulates endothelial cell migration during embryonic angiogenesis. Genes Dev 2007;21:2055–2068. [PubMed: 17699752]
15. Westerfield, M. The Zebrafish Book. Vol. 4 ed.. Eugene: University of Oregon Press; 2000.
16. Kimmel CB, Ballard WW, Kimmel SR, Ullmann B, Schilling TF. Stages of embryonic development of the zebrafish. Dev Dyn 1995;203:253–310. [PubMed: 8589427]
17. Bedell VM, Yeo SY, Park KW, Chung J, Seth P, Shivalingappa V, Zhao J, Obara T, Sukhatme VP, Drummond IA, Li DY, Ramchandran R. roundabout4 is essential for angiogenesis in vivo. Proc Natl Acad Sci U S A 2005;102:6373–6378. [PubMed: 15849270]
18. Stainier DY, Weinstein BM, Detrich HW 3rd, Zon LI, Fishman MC. Cloche, an early acting zebrafish gene, is required by both the endothelial and hematopoietic lineages. Development 1995;121:3141–3150. [PubMed: 7588049]
19. Cross LM, Cook MA, Lin S, Chen JN, Rubinstein AL. Rapid analysis of angiogenesis drugs in a live fluorescent zebrafish assay. Arterioscler Thromb Vasc Biol 2003;23:911–912. [PubMed: 12740225]
20. Lawson ND, Weinstein BM. In vivo imaging of embryonic vascular development using transgenic zebrafish. Dev Biol 2002;248:307–318. [PubMed: 12167406]
21. Sumanas S, Lin S. Ets1-related protein is a key regulator of vasculogenesis in zebrafish. PLoS Biol 2006;4:e10. [PubMed: 16336046]
22. Zhong TP, Rosenberg M, Mohideen MA, Weinstein B, Fishman MC. gridlock, an HLH gene required for assembly of the aorta in zebrafish. Science 2000;287:1820–1824. [PubMed: 10710309]
23. Lawson ND, Scheer N, Pham VN, Kim CH, Chitnis AB, Campos-Ortega JA, Weinstein BM. Notch signaling is required for arterial-venous differentiation during embryonic vascular development. Development 2001;128:3675–3683. [PubMed: 11585794]
24. Sugihara-Mizuno Y, Adachi M, Kobayashi Y, Hamazaki Y, Nishimura M, Imai T, Furuse M, Tsukita S. Molecular characterization of angiomotin/JEAP family proteins: interaction with MUPP1/Patj and their endogenous properties. Genes Cells 2007;12:473–486. [PubMed: 17397395]
25. Nagy JA, Dvorak AM, Dvorak HF. VEGF-A(164/165) and PlGF: roles in angiogenesis and arteriogenesis. Trends Cardiovasc Med 2003;13:169–175. [PubMed: 12837578]
26. Kaur S, Castellone MD, Bedell VM, Konar M, Gutkind JS, Ramchandran R. Robo4 signaling in endothelial cells implies attraction guidance mechanisms. J Biol Chem 2006;281:11347–11356. [PubMed: 16481322]

27. Wong K, Ren XR, Huang YZ, Xie Y, Liu G, Saito H, Tang H, Wen L, Brady-Kalnay SM, Mei L, Wu JY, Xiong WC, Rao Y. Signal transduction in neuronal migration: roles of GTPase activating proteins and the small GTPase Cdc42 in the Slit-Robo pathway. Cell 2001;107:209–221. [PubMed: 11672528]

28. Covassin LD, Villefranc JA, Kacergis MC, Weinstein BM, Lawson ND. Distinct genetic interactions between multiple Vegf receptors are required for development of different blood vessel types in zebrafish. Proc Natl Acad Sci U S A 2006;103:6554–6559. [PubMed: 16617120]

29. Estevez MA, Henderson JA, Ahn D, Zhu XR, Poschmann G, Lubbert H, Marx R, Baraban JM. The neuronal RhoA GEF, Tech, interacts with the synaptic multi-PDZ-domain-containing protein, MUPP1. J Neurochem. 2008

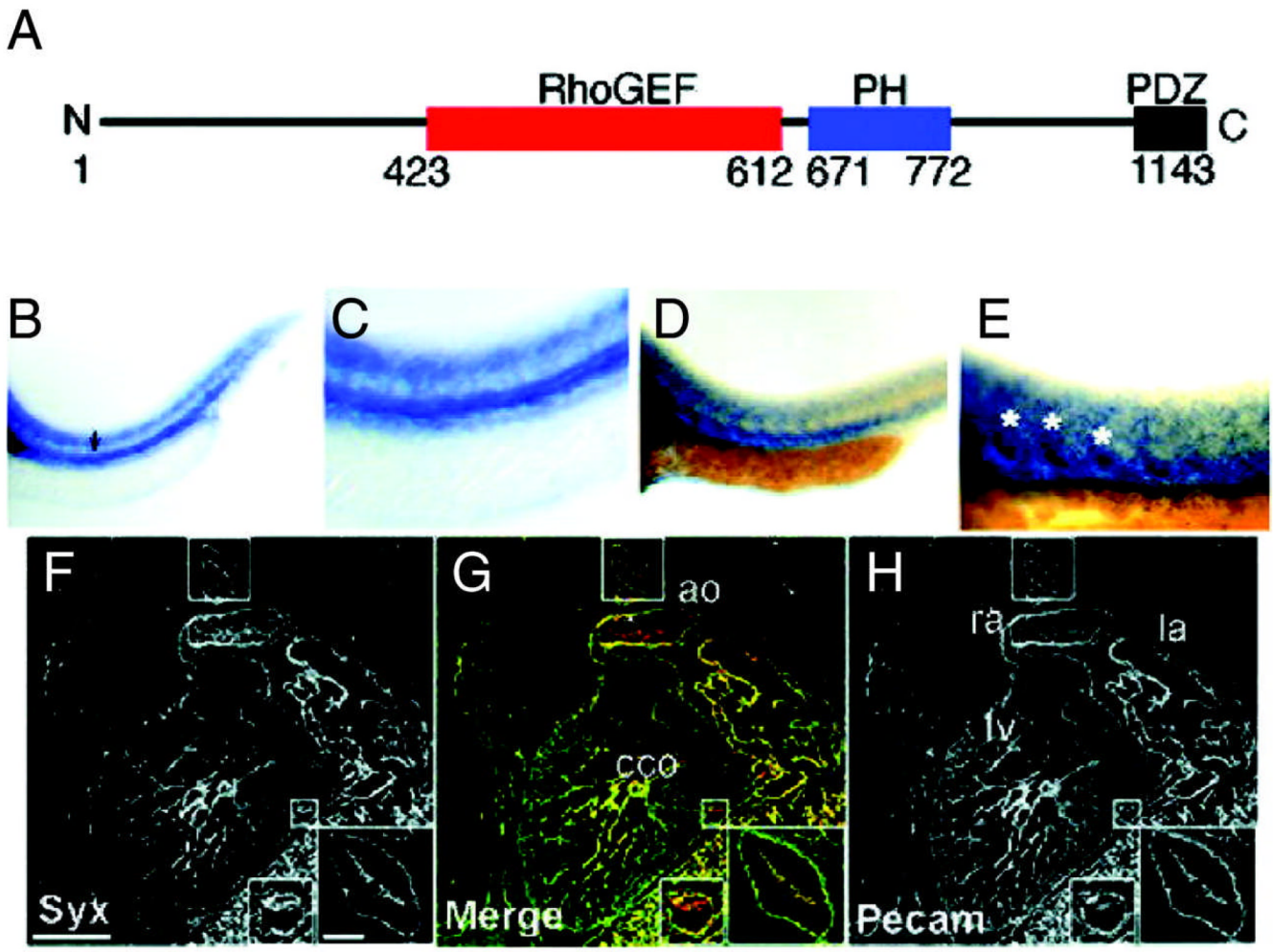

Fig. 1. *Syx* expression in zebrafish and mouse embryos

(A) The scheme shows the structure of the zebrafish Syx Rho-GEF (AA 423–612), Pleckstrin homology (AA 671–772) and a C-terminal PDZ-binding domain. (B–E) show whole mount *syx* ISH zebrafish embryos at 24 hpf in DA (B, black arrow) (C) sites of sprouting ISVs at 26 hpf (D, E asterisks). (F–H) Micrographs of an E12.5 mouse sagital section labeled with Syx and PECAM antibodies. The yellow-colored areas indicate merged image (G) indicates extensive co-localization of the two signals, which were originally red (Syx) and green (PECAM) (bars, 500 μm, 100 μm in inset). Insets are high power images of the aorta and circumflex coronary. ao: aorta, cco: circumflex coronary, la: left atrium, lv: left ventricle, ra: right atrium.

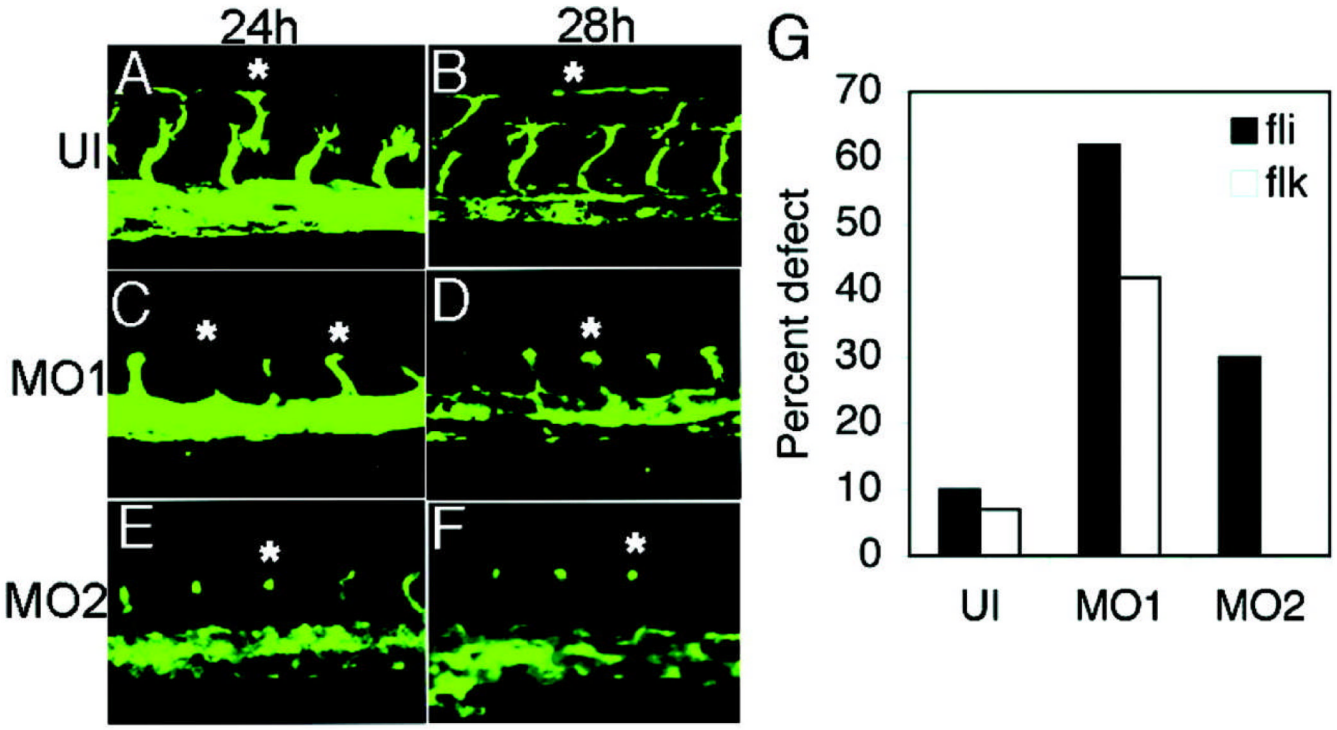

Fig. 2. *Syx* loss-of-function causes sprouting defects in zebrafish and mouse arteries

(A–F) are images of the trunk region of 24 hpf (A, C, E) or 28 hpf (B, D, F) Tg(*fli1*: EGFP) embryos. Panels (A, B) are uninjected (UI) embryos, (C, D) and (E, F) are age-matched MO1- and MO2-injected embryos, respectively. *Syx* KD embryos show truncated (C, asterisk) and knotted ISVs (D–F, asterisks). (G) is a graphical representation of percent defective embryos (*y*-axis) at 24 hpf: 63% (n = 41) of MO1-injected, 38% (n = 80) of MO2-injected, and 11% of UI (n = 47) Tg(*fli1*: EGFP) embryos show ISVs defects; 42% of MO1-injected Tg(*flk*: GRCF) embryos show ISVs defects compared to only 7% of UI embryos. Head is to the left.

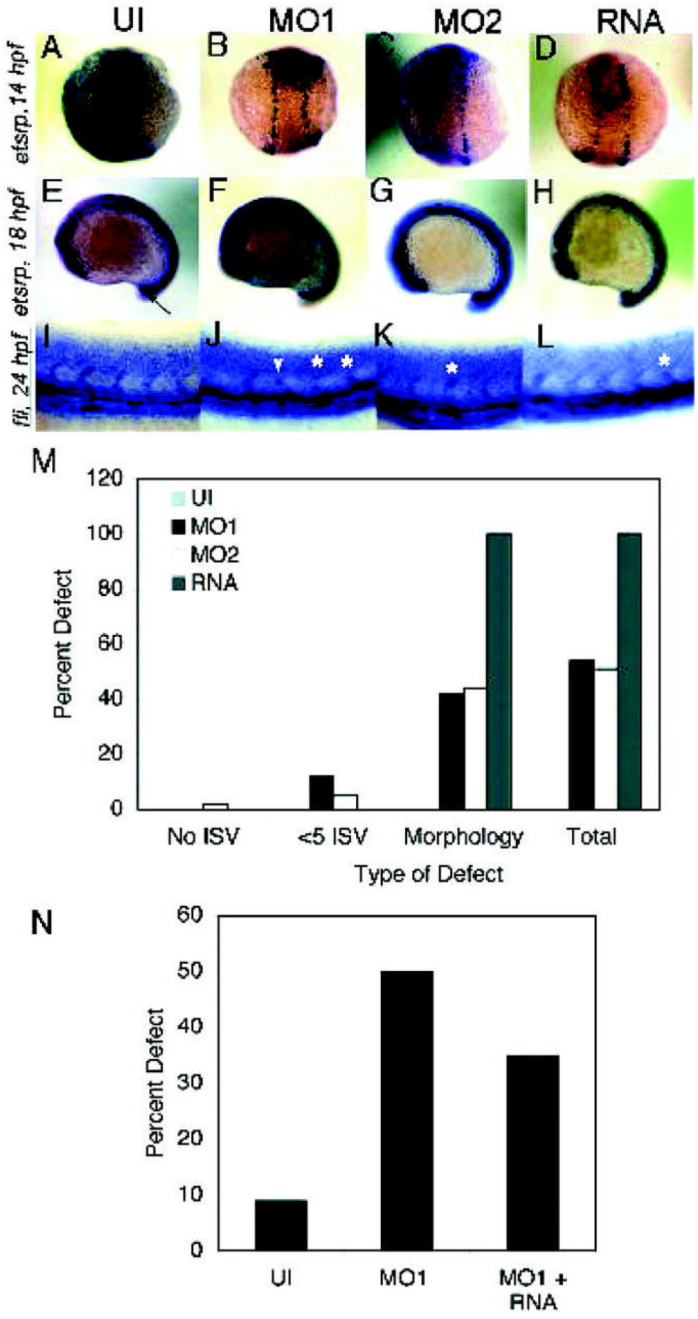

Fig. 3. *Syx* loss and gain-of-function embryos show similar defects

(A–L) show whole mount ISHs for *etsrp* at 14 hpf (A–D) and 18 hpf (E–H), and *fli* at 24 hpf (I–L). In 14 and 18 hpf *etsrp* ISH embryos, no distinct difference is noted across sample groups. At 24 hpf (I–L), truncated and/or blunt (asterisks) and misrouted ISVs (white arrowhead) are noted in MO- and RNA-injected embryos. (M) shows quantification of embryos (*y*-axis) displaying particular morphological defects (*x*-axis) observed in *fli* ISH embryos for each sample group. (N) shows percent defects (*y*-axis) in sample groups (*x*-axis): uninjected (UI, n=55), MO1-injected (MO1, n=42), or co-injected (MO1 + 200 pg *syx* mRNA, n=26) Tg (*fli1*: EGFP) embryos.

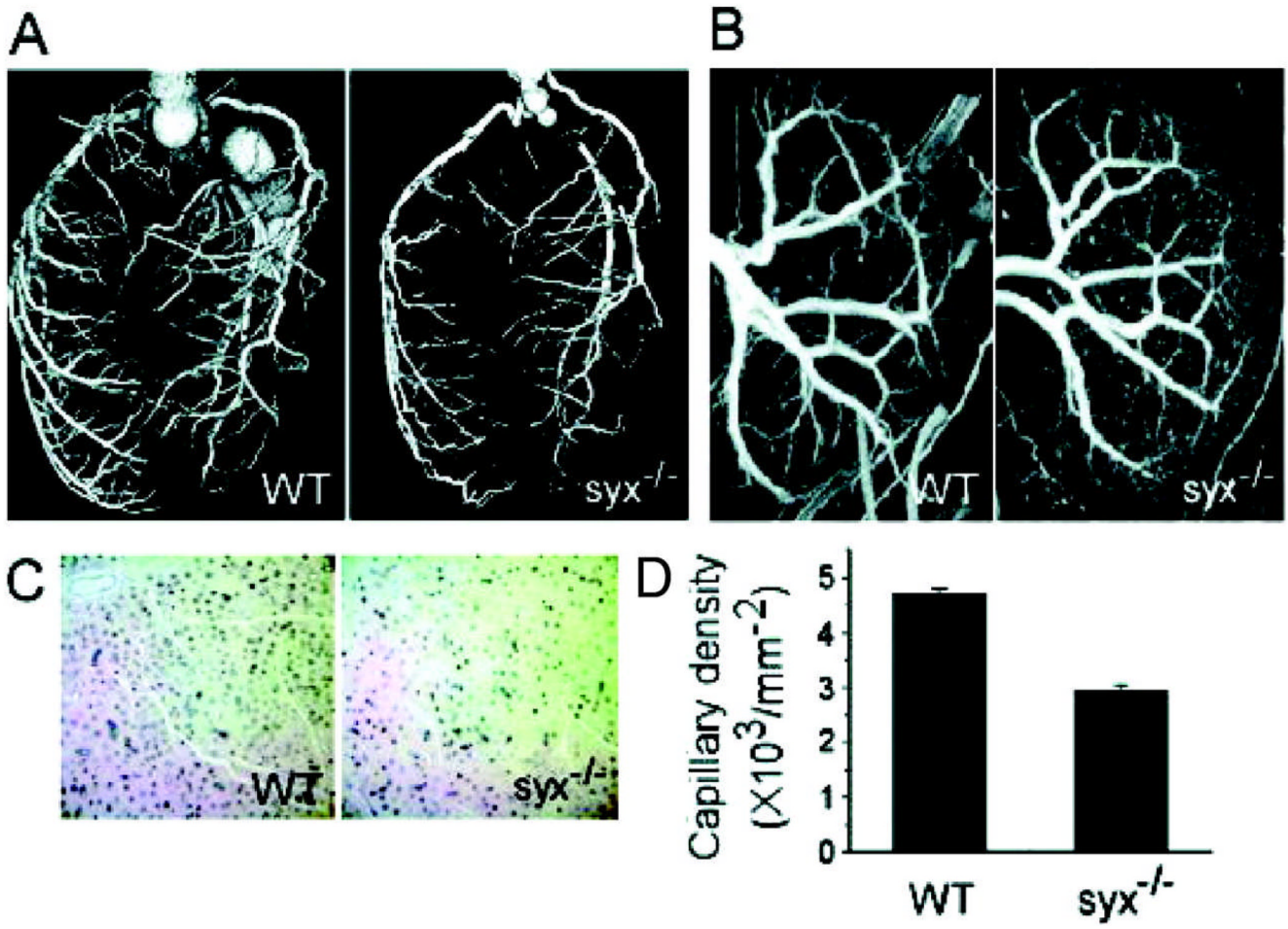

Fig 4. Vascular defects in *syx*$^{-/-}$ mouse

(A–B) show μCT image reconstructions of WT and *syx*$^{-/-}$ mouse arterial coronary vasculature (A) and kidney arterial vasculature (B). (C) Lectin-labeled sections of WT and Syx-KO myocardium (bar, 50 mm). (D) Capillary density in WT and *syx*$^{-/-}$ myocardia. Capillaries were counted in 4 sections, six 360×360 μm fields per section ($p<10^{-6}$).

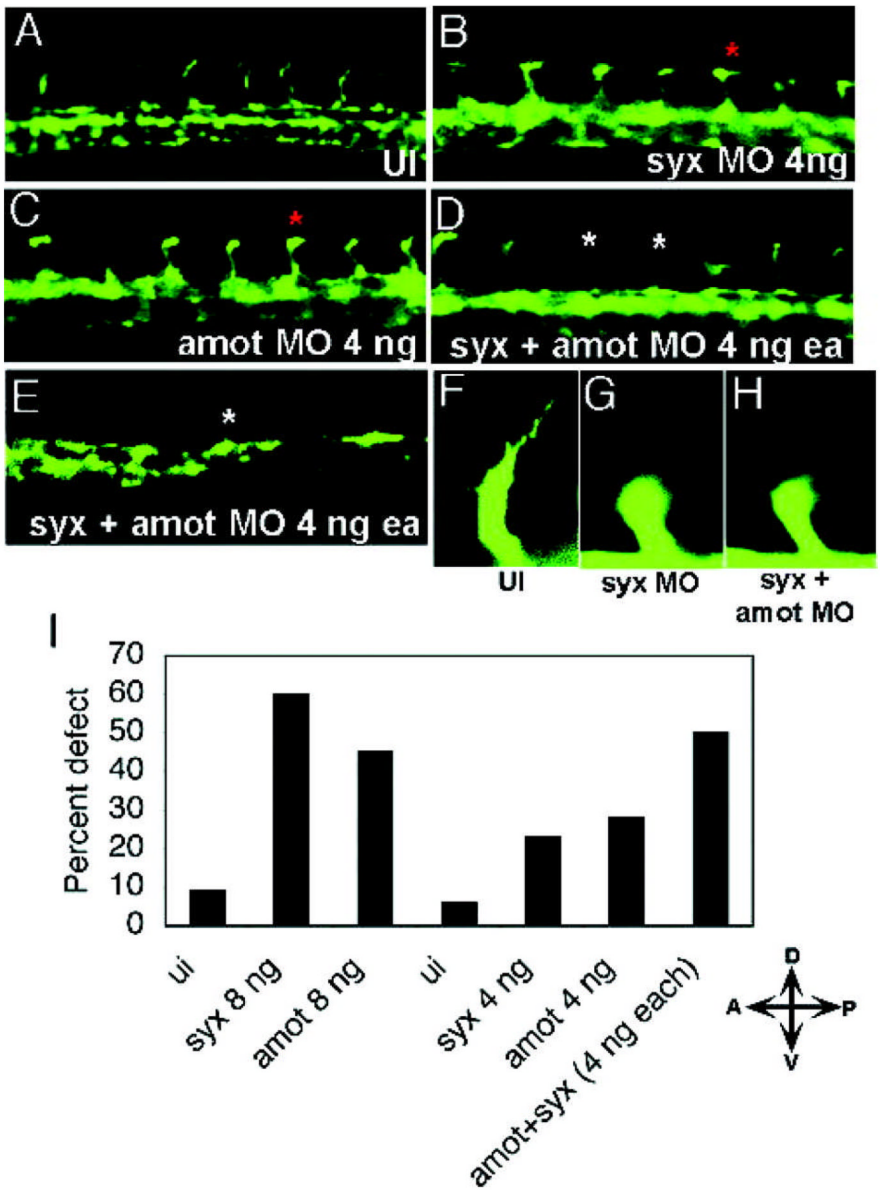

Fig. 5. Additive function for *amot* and *syx* in ISVs sprouting

(A–E) show the trunk region of Tg(*flk*: GRCFP) embryos at 28 hpf after injection with MOs indicated in the bottom right of each panel. The double-injected embryo in (E) displays complete absence of all ISVs. Red asterisks indicate truncated ISVs, and white asterisks indicate missing ISVs. (F–H) are high power trunk images of uninjected (UI), syx MO1-injected (syx MO), and syx MO- and Amot MO-injected (syx+amot MO) Tg(*flk*: GRCF) embryos. (I) is a graphical representation of the percent defective embryos (*y*-axis) within each sample group (*x*-axis) (ui: uninjected, n=46; syx 8 ng: *syx* MO 8 ng, n=42; amot 8 ng: *amot* MO 8 ng, n=56; ui: uninjected, n=17; *syx* 4 ng: *syx* MO 4 ng, n=22; *amot* 4 ng: *amot* MO 4 ng, n=18; *amot*+*syx* (4 ng each): *amot* MO 4ng + *syx* MO 4 ng, n=42). The compass indicates the orientation of the embryos.

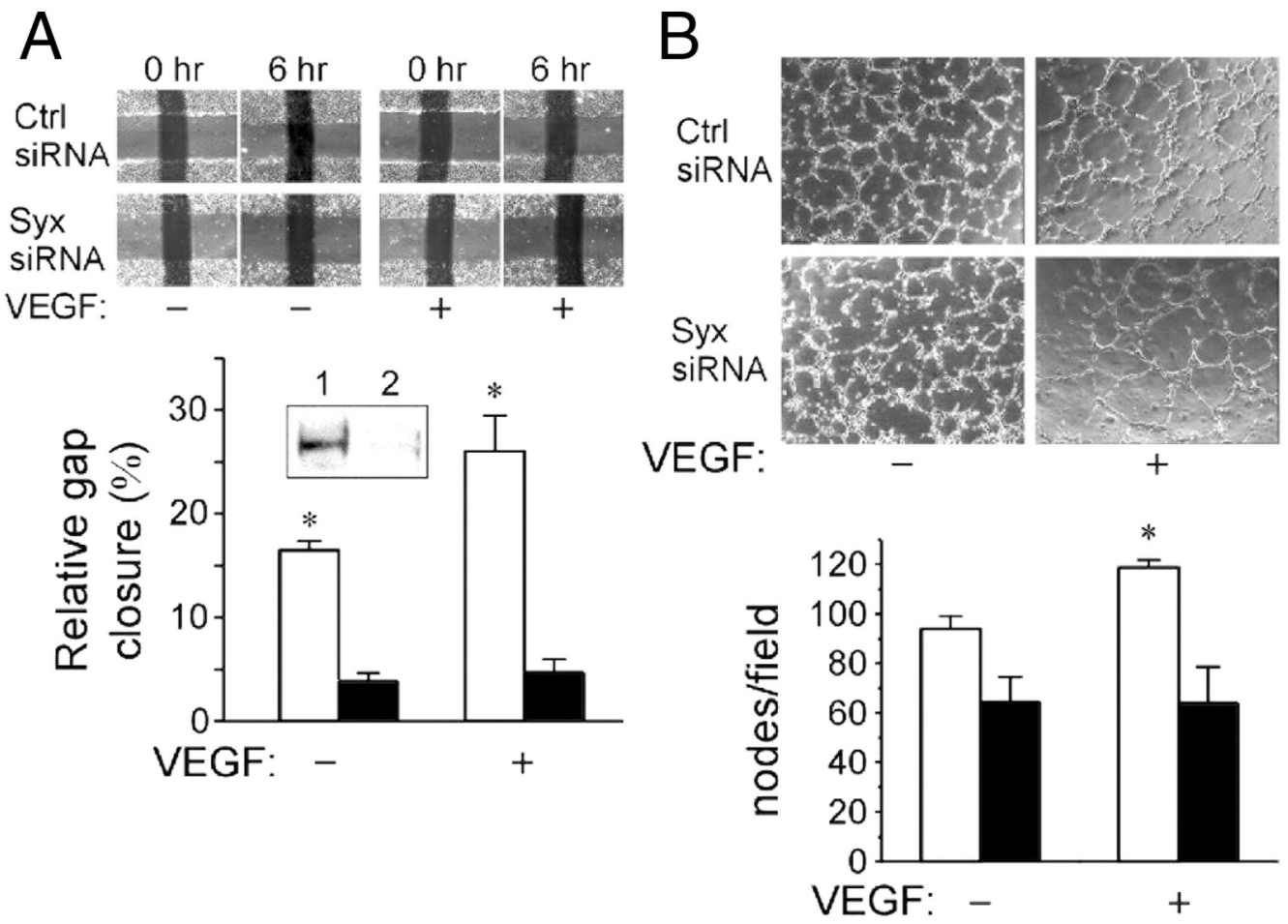

Fig. 6. ECs migration and *in vitro* tube formation assays

(A) Representative images of gap closure assays with rat fat pad ECs (RFPECs) transfected by the indicated siRNA, either with (+) or without (−) VEGF-A_{165} (50 ng/mL). The mean gap closure values are shown in the histogram. Black stripes were marked for measurement purposes. In the histogram, white and black bars represent control siRNA or *syx* siRNA-transfected ECs, respectively; n=3, ±S.D, $p<0.01$. The inset is an anti-Syx immunoblot of cell lysates from control siRNA (lane 1) or *syx* siRNA (lane 2)-transfected ECs. (B) Representative images of control or *syx* siRNA (lane 2)-transfected ECs. (B) Representative images of control or *syx* siRNA-transfected RFPECs grown on Matrigel with (+) or without (−) VEGF (50 ng). The mean number of nodes per field is shown in the histogram. White and black bars represent control siRNA or *syx* siRNA-transfected ECs, respectively; n=3, ±S.D, $p<0.03$.